Check for updates

ChemElectroChem

Research Article
doi.org/10.1002/celc.202500042

Chemistry Europe
European Chemical Societies Publishing

www.chemelectrochem.org

Effect of Operating Temperature on Ni–Fe Alloy Nanostructured Electrodes for Alkaline Electrolyzer

Alberto Affranchi, Roberto Luigi Oliveri,* Sonia Longo, Gabriele Micciché, Sonia Carbone, Francesca Bellomo, Salvatore Geraci, Bernardo Patella, Nadia Moukri, Giuseppe Aiello, Maurizio Cellura, Philippe Mandin, Myeongsub Kim, and Rosalinda Inguanta

Herein, the effect of operating temperature on alkaline electrolytic cells for hydrogen generation using nanostructured electrodes is studied. Nanostructured nickel–iron alloy electrodes are obtained by electrosynthesis in a template. These electrodes are characterized by a nanowire-like structure with a high active surface area and consequently a higher catalytic activity than non-nanostructured materials. The chemical and morphological features of nanostructured electrodes are evaluated by energy-dispersive spectroscopy, X-ray diffraction, and scanning electron microscopy analyses. The electrochemical behavior of the nanostructured electrodes is studied through different tests in alkaline solutions. Tests are performed at different temperatures, 25, 40, and 60 °C, to evaluate the performance in terms of hydrogen and oxygen production and to verify the medium-term stability under galvanostatic conditions. The electrodes demonstrate good stability over time without evident signs of performance decay. The performance of a homemade electrolyzer with nanostructured electrodes is also studied at different temperatures and under industrial operation conditions for 600 h. The environmental impacts through the application of life cycle assessment methodology are also evaluated.

1. Introduction

Hydrogen production through water splitting coupled with renewable energy sources, such as solar energy, is a promising strategy[1,2] to make hydrogen the main energy carrier of the future.[3] Renewable-powered water electrolysis represents one of the most advanced and promising technologies for the production of green hydrogen, which is a crucial component in the development of a sustainable energy system.[4,5,6] However, a major challenge remains—making these systems economically viable on a large scale. It is essential to work to increase the efficiency and stability of the system and to reduce the hydrogen production cost.[7,8] Many researchers are working on the development of catalysts for the oxygen and hydrogen evolution reactions (OER and HER, respectively) that offer both high efficiency and low cost, utilizing nonprecious and earth-abundant transition metals.[9] Nickel and its alloys, such as NiFe[10–12] and NiCo,[13] have received much attention due to their low cost, high activity for HER and OER, and good electrochemical stability. It is well established that the Ni–Fe alloy exhibits superior catalytic activity for the OER compared to pure Ni. However, under industrial operating conditions (60–80 °C and high current density), Fe leaching has been observed,[14–16] which must be addressed as it compromises the structural stability of the Ni–Fe alloy. Consequently, there is a strong need to enhance the operational stability of Ni–Fe alloy catalysts for industrial applications.

Research into electrode materials, with a particular focus on nanostructured materials, has resulted in significant advancements in the energy efficiency and stability of alkaline electrolyzers. Nanostructured catalysts provide a high number of active sites, enhancing electrochemical performance compared to their bulk counterparts.[17,18] In addition, electrocatalysts with nanostructured morphology exhibit good electronic conductivity and facilitate the rapid detachment of gas bubbles from the surface.[19] However, it should be noted that the overall performance of an alkaline electrolyzer is not solely determined by the quality of the electrocatalysts. The temperature of the electrolyte solution is a crucial factor, influencing critical parameters such as reversible voltage, reaction kinetics, ionic conductivity, and material stability. Industrial alkaline electrolyzers typically operate in

A. Affranchi, M. Cellura
Center of Sustainability and Ecological Transition
University of Palermo
Piazza Marina 61, Palermo 90133, Italy

R. L. Oliveri, S. Longo, G. Micciché, S. Carbone, F. Bellomo, S. Geraci, B. Patella, N. Moukri, G. Aiello, M. Cellura, R. Inguanta
Department of Engineering
Università degli Studi di Palermo
Viale delle Scienze, Palermo 90128, Italy
E-mail: robertoluigi.oliveri@unipa.it

P. Mandin
Université de Bretagne Sud
Institut de Recherche Dupuy de Lôme
IRDL UMR CNRS 6027, Lorient 6027, France

M. Kim
Department of Ocean and Mechanical Engineering
Department of Biomedical Engineering
Florida Atlantic University
777 Glades Rd., Boca Raton 33431, FL, United States

Supporting information for this article is available on the WWW under https://doi.org/10.1002/celc.202500042

© 2025 The Author(s). ChemElectroChem published by Wiley-VCH GmbH. This is an open access article under the terms of the Creative Commons Attribution License, which permits use, distribution and reproduction in any medium, provided the original work is properly cited.

© 2025 The Author(s). ChemElectroChem published by Wiley-VCH GmbH

21960216, 0, Downloaded from https://chemistry-europe.onlinelibrary.wiley.com/doi/10.1002/celc.202500042 by University Degli Studi Di, Wiley Online Library on [26/06/2025]. See the Terms and Conditions (https://onlinelibrary.wiley.com/terms-and-conditions) on Wiley Online Library for rules of use; OA articles are governed by the applicable Creative Commons License

the range from 40 to 90 °C.[20–23] Therefore, the electrodes used must be able to withstand these temperatures.

Researchers generally focus on the performance of electrocatalysts at ambient temperature. However, as demonstrated in another study,[24] neglecting the effect of temperature variations can lead to misleading conclusions. Some mathematical models have been proposed to describe the behavior of an alkaline electrolysis cell at different temperatures.[25–27] As expected, both theoretical models and experimental data indicate that increasing temperature leads to a decrease in cell voltage, thereby reducing the energy demand of the electrolyzer. Some authors have shown, however, that temperature affects different electrocatalysts differently. In Ref. [28] it was demonstrated that the performance of NiO*x* catalysts improves as the temperature increases from 25 °C to 50 °C. Zhang et al.[29] observed that the OER performance of Co-based catalysts peaks at a temperature range of 55–65 °C. This behavior was attributed to the change of the rate-determining step (RDS) from only OH^- adsorption to a mixed mode, where both adsorption and the cleavage of the OH group can be rate determining, resulting in faster kinetics. In Ref. [30] it was demonstrated that for NiCo/oxide materials, the ORR kinetic increases as the operating temperature increases from 20 to 80 °C and that this increase is particularly relevant (3 to 8 times higher) in the case where the catalyst is amorphous or poorly crystalline.

Considering that electrodes with nanowire morphology remain relatively underexplored, this article analyzes the influence of temperature on the performance of nanostructured electrodes, highlighting the implications for the overall efficiency of electrolyzer systems and identifying strategies to increase hydrogen production through optimal control of operating parameters. In particular, building on findings from previous works,[10,31] nanostructured NiFe electrodes were tested in 30 wt% aqueous potassium hydroxide solution at different temperatures to study their mechanical and chemical stability and validate their use in an industrial electrolyzer. These electrodes were fabricated using template electrodeposition in a polycarbonate template to obtain electrodes with nanowire morphology. Electrocatalysts produced through this method typically demonstrate enhanced structural stability and superior conductivity in comparison to those fabricated via alternative methodologies.[32,33] This approach eliminates the need for binders, ensuring strong adhesion between the active catalytic materials and the substrate thus reducing the catalyst detachment during electrocatalytic reactions.

In addition, the in situ growth of electrocatalysts in templates by electrodeposition provides two main advantages. First, it significantly increases the surface area of the electrocatalysts, exposing a greater number of active reaction sites. This enhances electrolyte penetration and facilitates gas bubble formation and detachment. Second, it improves electrical conductivity, further enhancing catalytic performance.[34] In addition to high catalytic activity, a cost-effective synthesis approach is a crucial factor for large-scale practical applications of electrocatalysts. A comparison of electrodeposition with alternative methods reveals several advantages, including the capacity to produce at ambient temperature, a reduced deposition time, and the ability to regulate the composition of electrocatalysts.[35] Therefore, electrodeposition shows strong potential for industrial production of efficient catalysts for water splitting.

The performance of nanostructured electrodes was studied using different electrochemical tests, including cyclic voltammetry (CV), quasisteady state polarization (QSSP), galvanostatic step (GS), and galvanostatic measurements at different temperatures (25, 40, and 60 °C) for both HER and OER. In addition, medium-term stability under galvanostatic conditions was also evaluated. The performance of a homemade alkaline electrolysis cell incorporating nanostructured electrodes was also studied at different temperatures to evaluate its efficiency and the impact of temperature on electrode morphology and stability in a flow cell. Finally, a life cycle assessment (LCA) was conducted to assess the energy and environmental impacts of the electrodeposition method and the entire electrolysis cell, employing a cradle-to-gate approach, to identify potential areas for improvement and provide reliable support to industrial decision-makers and product developers in an ecodesign perspective.[36] Additionally, the effect of heating the electrolyte (aqueous potassium hydroxide solution) over a 6-hour operation period was examined.

2. Results and Discussion

2.1. Materials and Methods

Nanostructured Ni–Fe electrodes were obtained by template electrodeposition. This method is a very simple and inexpensive as it can be performed at room temperature. The morphology of the electrodes depends mainly on the template used. In this study, a porous polycarbonate membrane (Whatman) was used. These membranes are characterized by a pore density of 10^{12} pore m^2, a pore diameter of 200–250 nm, and a thickness of 20 μm. The porous structure facilitates the formation of cylindrical nanostructures referred to as nanowires (NWs) during the electrodeposition process. To proceed with the electrodeposition process, the membrane must first be made conductive. A thin gold film (about 30 nm thick) is deposited on one side of the membrane via sputtering process by applying a continuous current of 30 mA for 3 min. The sputtering process was carried out using a Scancoat Six Sputter Coater from Edwards Ltd. After the sputtering process, a compact layer of nickel was electrodeposited onto the gold-coated surface of the membrane. This layer provides mechanical stability to the electrode and serve as a current collector, ensuring electrical connectivity across all the NWs that subsequently grow within the membrane pores. The solution used for the deposition of the nickel collector is the typical Watt's bath (300 g L nickel sulfate hexahydrate $NiSO_4 \times 6H_20$, 45 g L nickel chloride hexahydrate $NiCl_2 \times 6H_2O$, 45 g L boric acid H_3BO_3). Deposition takes place in a standard three-electrode cell configuration where the gold-coated membrane is the working electrode, a platinum mesh is the counter electrode, and the reference electrode is the calomel (SCE, 0.241 V vs. standard hydrogen electrode (SHE)). The Ni collector is obtained by potentiostatic electrodeposition at a potential of −1.5 V versus SCE for 90 min. The typical current pattern during the deposition is shown in

© 2025 The Author(s). ChemElectroChem published by Wiley-VCH GmbH

Figure S1a, Supporting Information. Once the electrodeposition of the Ni collector has been completed, the following step is the NWs electrodeposition. The solution used is the Watt's Bath, which also contains 0.44 M $FeSO_4 \times 7H_2O$. This composition has been chosen based on experimental data from previous research studies.[10] NWs were obtained by applying a square-wave pulsed electrodeposition with the potential values switched between −0.65 V versus SCE and −1.35 V versus SCE for 100 cycles. The two potentials were maintained for 4 s and 6 s, respectively. Figure S1b, Supporting Information shows the typical trend of potential and current density during the electrodeposition process of the NWs. The final stage of the process involves etching the membrane in four successive baths of five minutes each in pure chloroform.

2.2. Electrode Characterization

Before carrying out electrochemistry tests, electrodes were characterized by scanning electron microscopy (SEM) with a FEG-ESEM microscope (QUANTA 200 by FEI) and energy-dispersive spectroscopy (EDS) to evaluate the morphology and composition of the NWs. In addition, X-ray diffraction (XRD) analysis was performed using a RIGAKU X-ray diffractometer (D-MAX 25600 HK) in the 2θ range from 3° to 100°. Performance was evaluated in a three-electrode configuration. Instead the conventional test performed in 1 M KOH at room temperature, here a concentrated 30 wt% OH electrolyte was employed at different temperatures. Using the concentrated electrolyte at elevated temperature allows for the observation of possible corrosion processes and other degradation phenomena which can be negligible at low temperature. The electrodes were tested using different electrochemical tests in 30 % wt KOH aqueous solution. The electrode performance was evaluated at three temperature values (25 °C, 40 °C, and 60 °C), since this parameter significantly influences the system response.[23,24] The electrochemical tests were conducted in a three-electrode cell configuration, where the NiFe NWs electrode is the working electrode ($A \approx 0.6\ cm^2$), a nickel strip is the counter-electrode and a Hg/HgO electrode was used as reference. All the potential values were referenced to reversible hydrogen electrode (RHE). The performance of the bifunctional electrocatalyst was also studied in a lab-scale electrolyzer with a two-electrode configuration. A customized PMMA electrochemical flow cell was used. In a typical experiment, NiFe NWs ($2 \times 2\ cm^2$) electrodes were used as cathode and anode (NiFe NWs | NiFe NWs). The two electrodes are separated by a commercial separator (AGFA's ZIRFON) and immersed in 30 wt% KOH electrolytes. The performance of the lab-scale electrolyzer was evaluated under industrial-relevant conditions, which involved testing at the temperatures of 25, 40, 60, and 80 °C using a 30 wt% KOH electrolyte for several days.

All electrochemical tests were repeated three times using new electrodes obtained with identical deposition conditions. These tests were performed using a Cell Test System (Solartron, Mod. 1470 E, 8 channels). Data were recorded by a desk computer via MultiStat Software (Mod. UBS147010ES).

2.3. Life Cycle Assessment

The LCA analysis was carried out following the international LCA standards employing an attributional approach. The aims of the study are: to calculate the environmental impacts of the entire cell; to identify the main environmental hotspots through a contribution analysis; and to evaluate the environmental burdens/benefits of heating the electrolyte with electric energy at three different operating temperatures, 25 °C (room temperature), 40 °C, and 60 °C. A cradle-to-gate approach is adopted, including the life cycle stages from raw material extraction to the end of manufacturing, considering one cell as a functional unit. The calculation methodology is based on the EN 15 804 + A2 method.[36]

2.4. Electrochemical Testing

Electrocatalyst activities are strongly dependent on the active surface area for the reactions involved in water electrolysis. To evaluate the active surface area and the advantages of nanomorphology, CV tests have been performed on both planar and nanostructured electrodes. In particular, the double-layered capacitance (CDL)[37] was measured at different scan rates. From the CDL it is possible to estimate the electrochemically active area involved in electrochemical reactions. This is particularly useful for studying porous materials or catalysts, where the real surface area can significantly differ from the geometric area.[38] This is important because nanostructured materials often exhibit a much larger effective surface area due to their morphology, which enhances their catalytic performance by providing more active sites for reactions. CV was performed in a non-Faradaic region, ranging from 0.64 to 0.74 V versus RHE (Figure S2, Supporting Information) at different scan rates from 10 to 35 mV s^{-1}. For each scanning rate, the difference between anodic and cathodic current density at 0.7 V versus RHE was computed and then plotted against the scan rate. The slope of the linear fit is the double-layer capacitance.[39] The linear fit is shown in **Figure 1**. The slope of NiFe is much greater, about 7 times, than that of the Ni planar strip. This difference in current density can be explained by the difference in electrochemically active surface area between the planar Ni electrode and the nanostructures. This is a good result imputable to the very large surface area

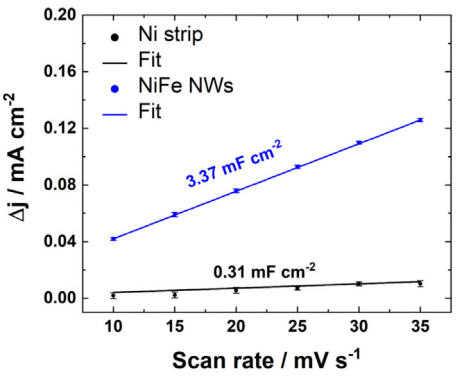

Figure 1. Specific capacitance of the electrodes evaluated by double-layer capacitance method: black) Ni strip; blue) NiFe NWs.

© 2025 The Author(s). ChemElectroChem published by Wiley-VCH GmbH

21960216, 0, Downloaded from https://chemistry-europe.onlinelibrary.wiley.com/doi/10.1002/celc.202500042 by University Degli Studi Di, Wiley Online Library on [26/06/2025]. See the Terms and Conditions (https://onlinelibrary.wiley.com/terms-and-conditions) on Wiley Online Library for rules of use; OA articles are governed by the applicable Creative Commons License

of the NWs.[40,41,42] Thus, on the NW electrode surface, there will be a greater evolution of the two gases as the OER and HER reactions are strongly dependent on the specific area. However, care should be taken to blindly use these values as real concentrations of active sites for the HER and OER. This is especially the case for porous support such as NWs as the measured CDL is influenced by many other phenomena that can alter the reliability of the obtained values.[43] QSSP, was performed in the potential range of 0.7 V around the thermodynamic potential of HER and OER. Tests were performed at 25 °C, 40 °C, and 60 °C for both HER (Figure S2a, Supporting Information) and OER (Figure S2b, Supporting Information). The increase in temperature led to a significant impact on the values of current density, as evidenced by experimental observations. Indeed, it is well established that an increase in temperature leads to an increase in both the conductivity of the electrolyte and the kinetics of the electrode reactions.[44,45]

Figure S2, Supporting Information shows that an increase in temperature has a significant impact on the reduction of Ohmic losses, which are predominant at high densities. Indeed, at low current densities, a closer alignment of the curves is evident. Conversely, a marked divergence between the curves becomes evident at elevated current densities. It is evident that current density increases with temperature, reaching a maximum at 60 °C under constant applied potential. QSSP were performed on three different electrodes obtained in the same deposition conditions to verify the reproducibility of the fabrication method. The curves obtained are practically superimposable and thus the reproducibility is quite strong.

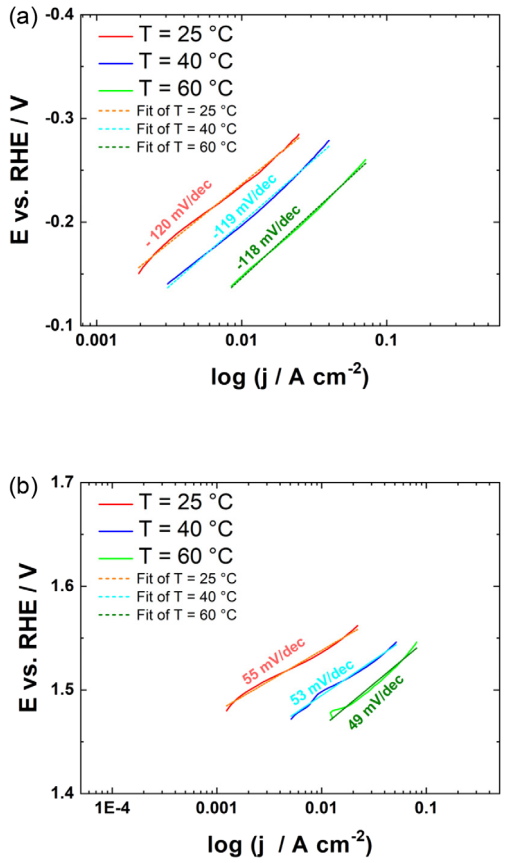

Figure 2. Linear range of QSSP for a) HER and b) OER.

Table 1. Fitted Tafel's parameters.

Temperature	HER			OER		
	a [V]	b [V dec]	R^2 [%]	a [V]	b [V dec]	R^2 [%)]
25 °C	−0.47	−0.120	99.17	1.62	0.055	99.6
40 °C	−0.44	−0.119	99.6	1.56	0.053	98.7
60 °C	−0.41	−0.118	99.8	1.55	0.049	99.1

To examine the kinetics for HER and OER, Tafel plots were constructed, **Figure 2**a,b, performing a linear regression analysis from which the characteristic parameters (a and b) of Tafel's equation were obtained. The Tafel's slopes at different experimental temperatures for HER and OER, are reported in **Table 1**. For both HER and OER, minimal variation among the different temperatures was found. The moderate change in Tafel slopes indicates that, in the interval of investigated temperatures, the RDS remains unchanged.[24] In Table S1, Supporting Information for comparison, the more relevant and recent literature data were reported. It can be observed that our results are very close to, and in some cases better than, those obtained by other authors. The slope values for HER approximate 120 mV dec, suggesting that the RDS of the reaction is the Volmer step. For the OER, a slope value of 55 mV was determined. This outcome is analogous to those attained with NiFe alloy electrodes. Table S1, Supporting Information also reports the overvoltage values at a current density of 10 mA cm^2, which is the accepted benchmark parameter for the comparison between HER and OER electrocatalysts.[46] Also in this case, the NiFe NWs electrodes show performances comparable or superior to those reported in the literature. The good electrocatalytic performance of Nife NW-based electrodes can be attributed to their elevated electrochemical active surface area, which ensures a substantial number of active sites for HER and OER. The GS test was performed to evaluate the behavior of electrodes at different current densities. The test was carried out using multiple current steps (10, 20, 50, 100, 200, and 500 mA cm^{-2}), each lasting 300 s.

Tests were conducted at varying temperatures to assess the electrode response in terms of potential for both reactions. Plotting the mean potential value obtained for each step on the corresponding current values yields a *J–V* plot (**Figure 3**) that is analogous to that obtained with the QSSP. For a given current value, the recorded potential decreases with increasing temperature, reaching a minimum for the curve corresponding to experiments performed at 60 degrees. Also, in this case, the reproducibility of the electrodes was verified using three different electrodes obtained in identical conditions. The very small amplitude of the error bars reported in Figure 3 suggests confirm the good reproducibility of the nanostructured electrode fabrication method. At a current of 100 mA cm^{-2}, the energy gain from 25 to 60 degrees is comparable to that reported in other studies.[47] Notably, applying a current density of 500 mA cm^{-2} significantly reduced overpotentials from −0.94 to −0.59 V versus RHE for HER

© 2025 The Author(s). ChemElectroChem published by Wiley-VCH GmbH

21960216, 0, Downloaded from https://chemistry-europe.onlinelibrary.wiley.com/doi/10.1002/celc.202500042 by University Degli Studi Di, Wiley Online Library on [26/06/2025]. See the Terms and Conditions (https://onlinelibrary.wiley.com/terms-and-conditions) on Wiley Online Library for rules of use; OA articles are governed by the applicable Creative Commons License

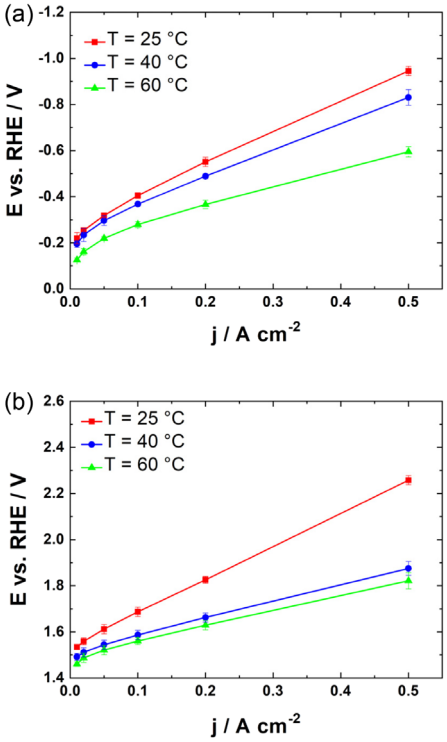

Figure 3. Galvanostatic step polarization for a) HER and b) OER.

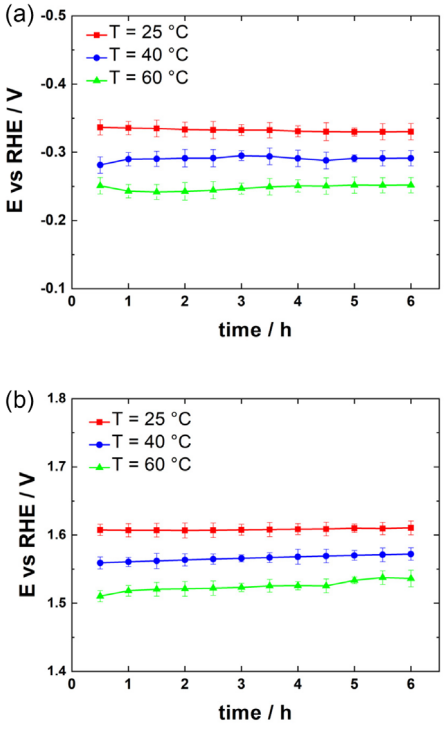

Figure 4. Midterm stability test for 6 h: a) HER at $-50\ mA\ cm^{-2}$ and b) OER at $+50\ mA\ cm^{-2}$.

and from 2.25 V to 1.82 V for OER. A reduction in the overpotential makes the process more energetically viable by reducing the energy required to operate the system while increasing its efficiency. GS polarization was also performed on different types of electrodes obtained by electrodepositing the NiFe catalyst, with identical deposition parameters, on nickel sheet (NS) and nickel foam (NF). These tests were carried out to assess the impact of the morphology of the NWs compared to the same alloy deposited on different substrates. The comparison (Figure S5, Supporting Information) shows that for the same geometric area, NWs perform better or are comparable to NFs and superior to NSs. Despite the noteworthy, electrocatalytic capabilities of Ni foams as substrates for electrocatalysts in water splitting applications, the utilization of metal foams is encumbered due to their high cost and low mechanical properties that hindered their use in zero-gap electrolyzers. In Table S2, Supporting Information the esteemed costs for the fabrication of different NiFe-based electrodes were reported. Based on laboratory-estimated cost, for NiFe NW-based electrodes, a cost of $\approx$0.27 € cm^2 was calculated. A comparison of this value with those calculated for the same alloy deposited on Ni foam and SS 316 substrates demonstrates the economic advantage of nanostructured electrodes with nanowire morphology obtained by template deposition technique.

To evaluate the stability of the electrodes, midterm stability tests were carried out. A possible degradation of electrode performance over time would result in an increase in cell voltage during the operating period. Thus, the galvanostatic tests were performed for six hours at a constant current density of $50\ mA\ cm^{-2}$ for the OER and $-50\ mA\ cm^{-2}$ for the HER at different operating temperatures, **Figure 4**. Each point on the graph represents the average potential recorded over 1800 s. A substantial decrease in recorded potential will be observed as the temperature rises, according to previously observed in the QSSP and GS results. The electrodes show excellent medium-term stability and reproducibility. For all investigated temperatures, the galvanostatic curves remain almost constant with negligible drops in potential. The best result was obtained in the test at the highest temperature, according to Nagai et al.[48] In particular, at 60 °C, there was a decrease in the potential of about 70 mV for HER and about 90 mV for OER compared to tests performed at room temperature.

After the test, the electrodes were tested at 60 °C and examined by SEM and XRD to evaluate their mechanical and chemical stability following several hours of operation. The results were then compared with those obtained before the electrochemical test. SEM images of the electrodes at increasing magnifications before the electrochemical test are shown in Figures S4a and S4b, Supporting Information. The NWs have a cylindrical structure and a smooth and regular surface, and they are evenly distributed over the entire surface of the nickel collector. Figure S4c, Supporting Information also shows a side view of the NWs, highlighting their length. The SEM measurement shows NWs with a length of about 17 μm, which suggests that the parameters defined during the electroplating process have promoted optimal growth of the structures. Since the production of hydrogen and oxygen is directly proportional to the catalytically active area of the electrode (i.e., longer NWs allow greater production of both gases), these length values are certainly a positive feature. To obtain the EDS spectrum measurement with a more accurate estimation of the composition, the NWs were stripped from the

© 2025 The Author(s). ChemElectroChem published by Wiley-VCH GmbH

21960216, 0, Downloaded from https://chemistry-europe.onlinelibrary.wiley.com/doi/10.1002/celc.202500042 by University Degli Studi Di, Wiley Online Library on [26/06/2025]. See the Terms and Conditions (https://onlinelibrary.wiley.com/terms-and-conditions) on Wiley Online Library for rules of use; OA articles are governed by the applicable Creative Commons License

nickel collector. Figure S4d, Supporting Information shows the EDS spectrum of the electrode where the presence of both nickel and iron was confirmed. As explained in the previous work,[10] although the NWs were obtained from a solution richer in nickel than in iron, the EDS spectrum confirms the anomalous behavior of Fe alloys, which produces NWs with a higher iron content, about 75%, despite being the least noble element present in solution. The inhibition of nickel deposition in the presence of iron is due to the preferential adsorption of intermediate iron species on the electrode surface[49,50] and the presence of complexing agents such as boric acid. In particular, the complex formed between nickel and boric acid is more stable than that formed between iron and boric acid and this slows/inhibits nickel deposition.[10,51]

After the OER and HER tests at 60 °C, the SEM images (**Figure 5**) revealed good stability of the electrodes. In both cases, the nanostructures remained perfectly preserved. The medium-high temperature did not damage the electrode morphology demonstrating outstanding stability of the electrocatalyst during the electrochemical test.

These results are very promising. The mechanical and electrochemical stability demonstrated by the electrode in the medium-high temperature tests allows us to consider possible applications of these electrodes in industrial alkaline electrolyzers operating at temperatures higher than room temperature.

After the galvanostatic test performed at 60 °C, nanostructured electrodes were also characterized by XRD (**Figure 6**). Peaks at ≈43.23°, 50.38°, 74.18° and 90.16° can be attributed to the (111), (200), (220) and (420) planes of the Fe–Ni fcc alloy (Board No. 47-105).[52,53] In addition, Ni peaks were observed at 44.53°, 51.86° and 76.37°. These are associated with the face-centered cubic α-Ni structure (table no. 04-850). XRD spectra remain practically unchanged after medium-term stability testing, confirming SEM results and thus the stability of the nanostructured NiFe electrodes.

Due to the good activities in OER and HER processes in alkaline media at different temperatures, the NiFe NWs electrocatalyst was applied as a bifunctional catalyst in a homemade scale-lab alkaline electrolyzer. The scheme of the water electrolysis cell

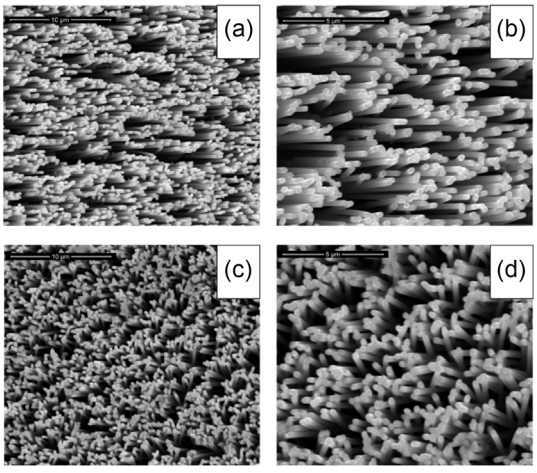

Figure 5. SEM images of NiFe NWs after galvanostatic test performed at 60 °C a)–b) HER; c)–d) OER.

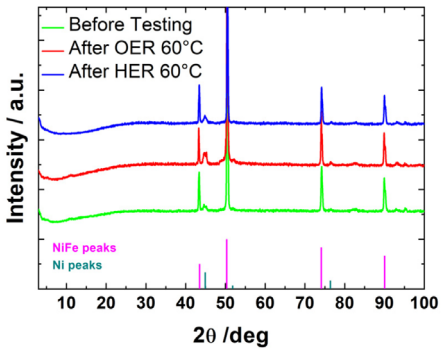

Figure 6. XRD pattern of NiFe NWs: green) before testing; red) after mid-term galvanostatic test OER at 60 °C; blue) after midterm galvanostatic test HER at 60 °C.

system is shown in **Figure 7**a. The system consists of an alkaline electrolyzer connected to a potentiostat to apply the desired current or potential, along with a pump that circulates the KOH solution, which is then recirculated through appropriate connections and heated by a heat exchanger.

A small-gap electrolysis cell (AE) with an effective active area of 4 cm^2, Figure 7b,c, was fabricated using polymethyl methacrylate (PMMA) plates which were designed and shaped with a laser cutter. Figure 7d shows the homemade prototype connected to the gas/liquid separator and temperature control system. Two Ni plates were used as current collectors, while NiFe NWs served as both the anode and cathode electrodes. A Zirfon diaphragm (Agfa Zirfon Perl UTP 500) was employed as a separator, and the gasket was made from polytetrafluoroethylene (PTFE) and shaped with a laser cutter. The electrolyte was circulated through the cell at a constant flow rate with the assistance of peristaltic pumps. To test the functionality of the system, several electrochemical tests were conducted, including QSSP, GS, and galvanostatic stability tests at three different temperatures, 25 °C. 40 °C and 60 °C. **Figure 8**. QSSP curves were obtained in the potential range 1.3–3 V at 10 mV s^{-1}. The GS curves replicate the trend of the QSSP curves. To reach a current density of 500 mA cm^{-2}, the potential required decreases from 3 V to 2.48 V, from 25 °C to 60 °C. To study the stability of the electrodes and the ability of the lab-scale electrolyzer to work for a continuous operation, a current density of 100 mA cm^{-2} was imposed at the beginning for 6 h. Each point on the graph represents the average recorded potential over 1800 s. After the first two hours, the potential reaches an approximately constant value for all investigated temperatures, measuring a decrease from 2.08 to 1.98 V for the test carried out at 25 °C and 60 °C, respectively. At 100 mA cm^{-2} after 6 h of testing, the values of cell potential are 1.99 V at 25°. 1.97 V at 45 °C and 1.9 V at 60 °C, with a decrease respect 25 °C of 3.4% and 2.2% at 60 °C and 40 °C, respectively. In the medium term, with minimal potential fluctuations, the curves remain largely constant.

Overall, the above results indicate the remarkable activity and stability of the NiFe NWs in alkaline conditions, which is critical for the large-scale application of electrocatalysts. Hence, the NiFe NWs are promising bifunctional electrodes for highly efficient alkaline water electrolyzers. The findings from this study indicate

© 2025 The Author(s). ChemElectroChem published by Wiley-VCH GmbH

21960216, 0, Downloaded from https://chemistry-europe.onlinelibrary.wiley.com/doi/10.1002/celc.202500042 by University Degli Studi Di, Wiley Online Library on [26/06/2025]. See the Terms and Conditions (https://onlinelibrary.wiley.com/terms-and-conditions) on Wiley Online Library for rules of use; OA articles are governed by the applicable Creative Commons License

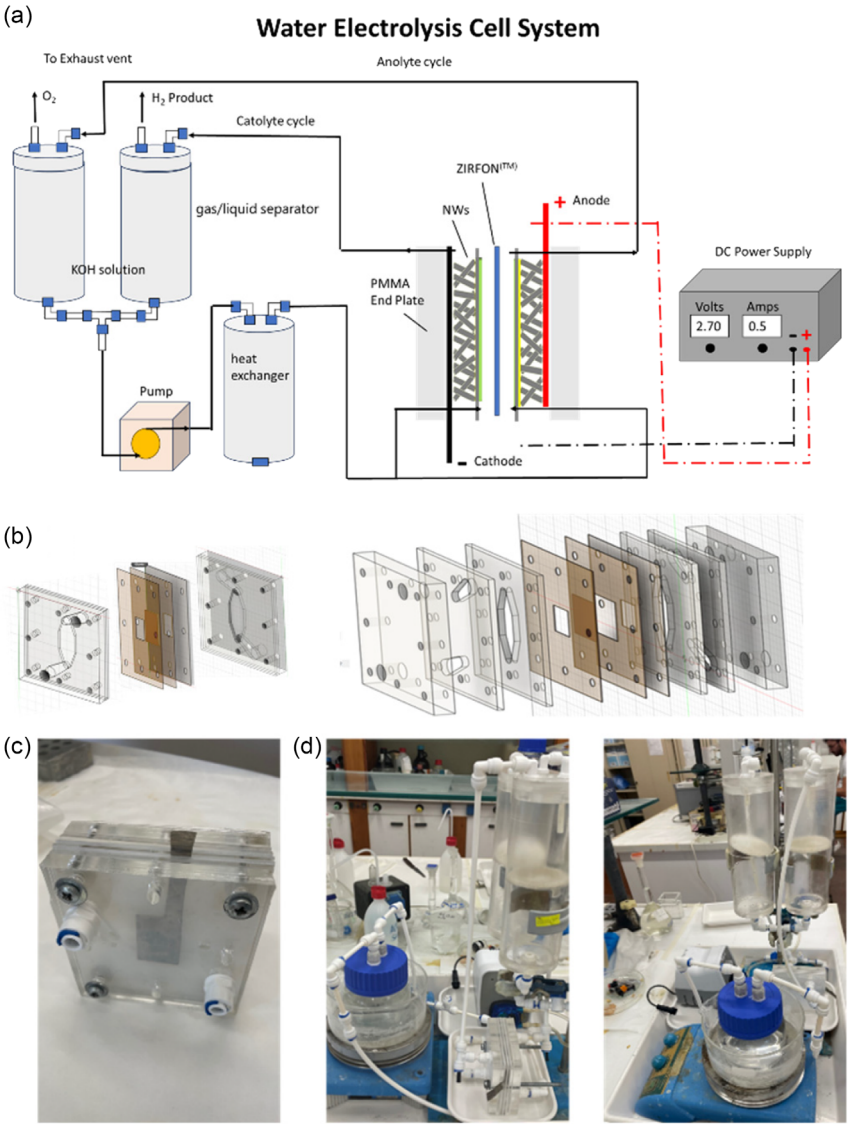

Figure 7. a) Scheme of the lab-scale electrolyzer system. b) Design and c) photograph of assembled electrolysis cell. d) Photograph of complete scale-lab alkaline electrolyzer.

that raising the operating temperature of alkaline electrolyzers can significantly enhance the device performance. As highlighted above, it is important to evaluate the performance of the developed electrocatalyst under industrial-relevant conditions to assess the possibility of practical application for NW electrodes. Thus, the NiFe nanostructured electrodes were tested by linear scanning polarization (LSV) and galvanostatic test for 125 h at 100 mA cm^{-2} at increasing temperatures up to 80 °C. The KOH aqueous solution reaches its maximum electrical conductivity at this temperature, significantly reducing the potential drop. **Figure 9**a reported the LSV curves obtained in the potential range 1.3–3 V at 10 mV s^{-1}. Of course, the best performance is reached at 80 °C. Maintaining high temperature is essential for industrial electrolysis, but it also places higher demands on the stability of the catalyst. Thus, the stability test was conducted for 125 h at a current density of 0.1 A cm^{-2} at increasing temperatures, followed by 5 min at the open circuit. As shown in Figure 9b, for each step at different temperatures, reasonable potential oscillations of ≈2% at 25 °C, 1.5% at 40 °C, 2.5% at 60 °C, and 3.8% at 80 °C are obtained. NiFe NWs demonstrate optimal industrial stability, running stably for a total of 600 h at 100 mA cm^{-2} in a 30% w/w KOH solution, demonstrating a promising outlook for industrial applications.

The morphology and surface composition of NiFe NWs after long-term galvanostatic tests were investigated by SEM and EDS. As evident from **Figure 10**, there are differences in surface morphology between the as-synthesized NiFe NWs, Figure S4, Supporting Information and after 600 h of electrolysis in 30 wt% KOH at increasing temperatures from 25 °C to 80 °C. The images indicate that the surface of the NWs used as anode has undergone an oxidation process. Nevertheless, EDS analysis revealed an absence of Fe leaching on the anode. The Fe content in the NWs persisted at 78% after 600 h of operation under industrial conditions. On the cathode (Figure 10c–d), however, the nanowire structure is still present, although a surface precipitate

© 2025 The Author(s). ChemElectroChem published by Wiley-VCH GmbH

21960216, 0, Downloaded from https://chemistry-europe.onlinelibrary.wiley.com/doi/10.1002/celc.202500042 by University Degli Studi Di, Wiley Online Library on [26/06/2025]. See the Terms and Conditions (https://onlinelibrary.wiley.com/terms-and-conditions) on Wiley Online Library for rules of use; OA articles are governed by the applicable Creative Commons License

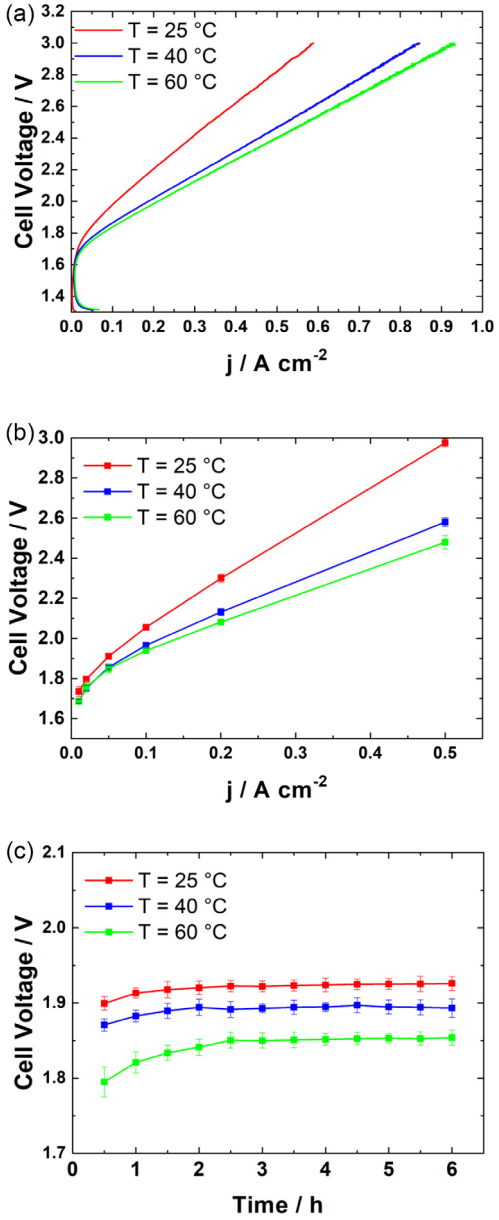

Figure 8. Electrochemical test carried out using lab-scale electrolyzer with NiFe NWs: a) QSSP, b) galvanostatic step polarization, c) midterm stability test.

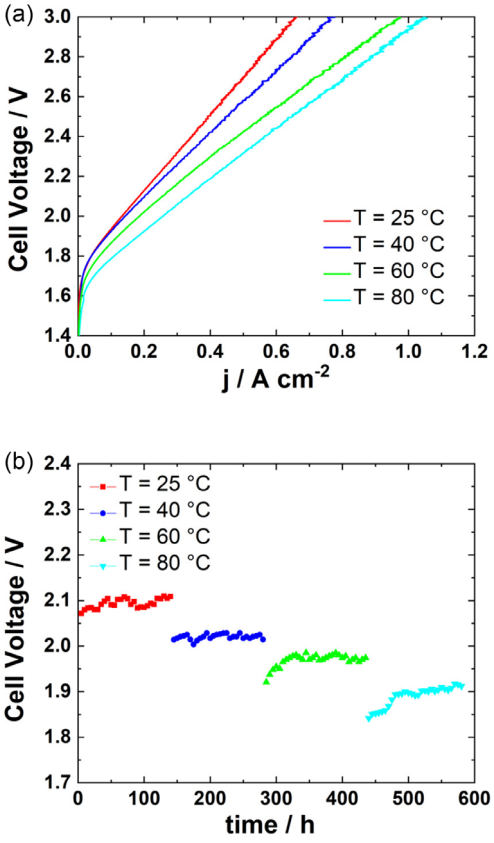

Figure 9. Electrochemical test carried out using lab-scale electrolyzer with NiFe NWs: a) LSV, b) cell voltage for galvanostatic step of 125 h at a current density of 0.1 A cm^2 at different temperature. Experiments were performed in 30 wt% KOH.

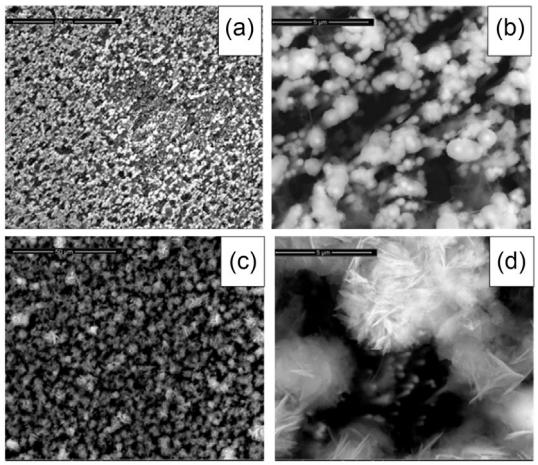

Figure 10. SEM images of the top view of NiFe NWs after 600 h in 30 wt% KOH at increasing temperatures from 25 to 80 °C (125 h each temperature). a–b) anode, c–d) cathode.

is observed. EDS analysis of the presence of oxygen due to the surface conversion in KOH solution, in addition to traces of Si, Ca, and Mg. The presence of these elements suggests that the electrolyte was contaminated by the silicone grease employed for the sealing of the flow cell. On the cathode side, no significant changes were measured in the Fe content, which remained at around 77%.

2.5. Application of the Life Cycle Assessment

LCA is an internationally recognized methodology based on UNI EN ISO 14040[54] and UNI EN ISO 14044[55] for calculating the potential energy and environmental impacts of products or services by analyzing their entire lifecycle. By examining the whole life cycle, LCA reveals hidden burdens and identifies opportunities for optimization from an ecodesign perspective. In this context, LCA plays a fundamental role in the scale-up process of emerging technologies by providing a comprehensive evaluation of the energy and environmental impacts across several impact categories. By systematically analyzing resource consumption,

© 2025 The Author(s). ChemElectroChem published by Wiley-VCH GmbH

21960216, 0, Downloaded from https://chemistry-europe.onlinelibrary.wiley.com/doi/10.1002/celc.202500042 by University Degli Studi Di, Wiley Online Library on [26/06/2025]. See the Terms and Conditions (https://onlinelibrary.wiley.com/terms-and-conditions) on Wiley Online Library for rules of use; OA articles are governed by the applicable Creative Commons License

21960216, 0, Downloaded from https://chemistry-europe.onlinelibrary.wiley.com/doi/10.1002/celc.202500042 by University Degli Studi Di, Wiley Online Library on [26/06/2025]. See the Terms and Conditions (https://onlinelibrary.wiley.com/terms-and-conditions) on Wiley Online Library for rules of use; OA articles are governed by the applicable Creative Commons License

emissions, and waste generation at different stages of the product or process life cycle, with its holistic approach, LCA enables to identify potential areas of improvement of the environmental and energy performances. Also, from the early stages of design, this approach identifies the hotspots (the life cycle stages or inputs that contribute most significantly to environmental impacts). By detecting these hotspots, the analysis allows to anticipate potential inefficiencies and environmental burdens before full-scale implementation, enhancing sustainability of emerging technologies in an ecodesign framework.

The LCA analysis is divided into four main phases. In the first phase, Goal and Scope Definition, the study delineates its objectives, system boundaries, functional units, allocation procedures, selected impact categories, and calculation methods. The next phase, Life Cycle Inventory Analysis, involves the collection and elaboration of data related to resource utilization, direct emissions, and waste generation. In the third phase, Life Cycle Impact Assessment, the environmental impacts are quantified based on the collected data and the methodology established in the previous phase. Finally, in the fourth phase, Life Cycle Interpretation, the results of the study are synthesized and analyzed to formulate recommendations and conclusions.

The inventory was obtained by examining the manufacturing process of the cell, which includes the lab-scale production of the NiFe electrodes, electrolytes, cell walls, gaskets, pumps, and pipes. The production process of the electrodes consists of three main phases; initially, a polycarbonate track-etched membrane (as a matrix for the nanowire conductors) is subjected to a sputtering process that deposits a thin layer of gold. Subsequently, electrodeposition forms the NiFe layer, and finally, trichloromethane etching dissolves the polycarbonate membrane. The other components were obtained through a direct analysis of the cell. All components and energy required for production are shown in **Table 2**. For secondary data, the environmental database Ecoinvent[56] was used. Specifically, the pump was derived from a proxy, the pipes and connectors are made of polypropylene, the gaskets are composed of polymethyl methacrylate, and then the 30% solution of KOH is prepared using potassium hydroxide and deionized water.

The results of the LCA analysis are presented in **Table 3**, referring to the functional unit of the cell.

For six categories, the components characterized by the highest environmental burden were the cell walls, with incidences of 31% for acidification, 37% for particulate matter, 36% for marine eutrophication, 31% for terrestrial eutrophication, 39% for photochemical ozone formation, and 40% for fossil resource use as shown in **Figure 11**.

The electrodes were responsible for the greatest environmental impact in five categories, with incidences of 35% for freshwater eutrophication, 40% for human carcinogenic toxicity, 49% for ionizing radiation, 65% for minerals and metals resource use, and 48% for water use. The pump and gaskets caused the most significant impact in two categories each: 58% for human noncarcinogenic toxicity, 28% for land use, 72% for climate change, and 62% for ozone depletion, respectively. The electrolyte was responsible for the greatest impact in only one category, freshwater ecotoxicity, with an incidence of 61%. The other components caused a negligible impact in almost all categories, with screws characterized by an average value of 4%, pipes and connectors by 2%, and Zirfon by less than 1% in all categories. In conclusion, the components responsible for the highest environmental burden in several categories were the cell walls and electrodes, while the gaskets and pump were significant in two categories each and the electrolyte in one category.

The results of the second objective of the study, which was to evaluate the effects of heating the electrolyte, are shown in **Table 4**. They are referred to the cell use over a 6 h operation period. The scenarios with 40° and 60° of temperature led to

Table 2. Inventory.

Component	Material	Quantity
Single electrode	Polycarbonate	28.1 mg
	Gold	1.6 mg
	Electrical energy	6.2 Wh
	$NiSO_4$	9 g L
	$NiCl_2$	1.35 g L
	$H3BO_3$	1.35 g L
	$FeSO_4$	0.1 g L
	Distilled water	0.03 L
	$CHCl_3$	0.1 L
Pump (2 W)	–	1 pc
Pipes and connectors	Polypropylene	82,02 g
Gaskets	Tetrafluoroethylene	95.4 g
Screws	Steel	159.2 g
Cell walls	Polymethyl methacrylate	266.8 g
Zirfon	–	1.2 g
Electrolyte	30% KOH solution	300 mL

Table 3. Impact assessment results.

Impact categories	Unit	Total impact
Acidification	mol H^+_{eq}	4.22 E-02
Climate change	kg CO_{2eq}	1.97 E+01
Ecotoxicity, freshwater	CTUe	1.15 E+02
Particulate matter	kg N_{eq}	3.45 E-07
Eutrophication, marine	kg P_{eq}	5.62 E-03
Eutrophication, freshwater	mol N_{eq}	2.34 E-03
Eutrophication, terrestrial	CTUh	5.65 E-02
Human toxicity, cancer	CTUh	3.56 E-08
Human toxicity, noncancer	kBq U-235_{eq}	2.02 E-07
Ionizing radiation	Pt	3.53 E-01
Land use	kg $CFC11_{eq}$	1.61 E+01
Ozone depletion	disease inc.	5.66 E-04
Photochemical ozone formation	kg $NMVOC_{eq}$	2.35 E-02
Resource use, fossils	MJ	8.92 E+01
Resource use, minerals and metals	kg Sb_{eq}	3.69 E-04
Water use	$m^3_{depriv.}$	2.43 E+00

© 2025 The Author(s). ChemElectroChem published by Wiley-VCH GmbH

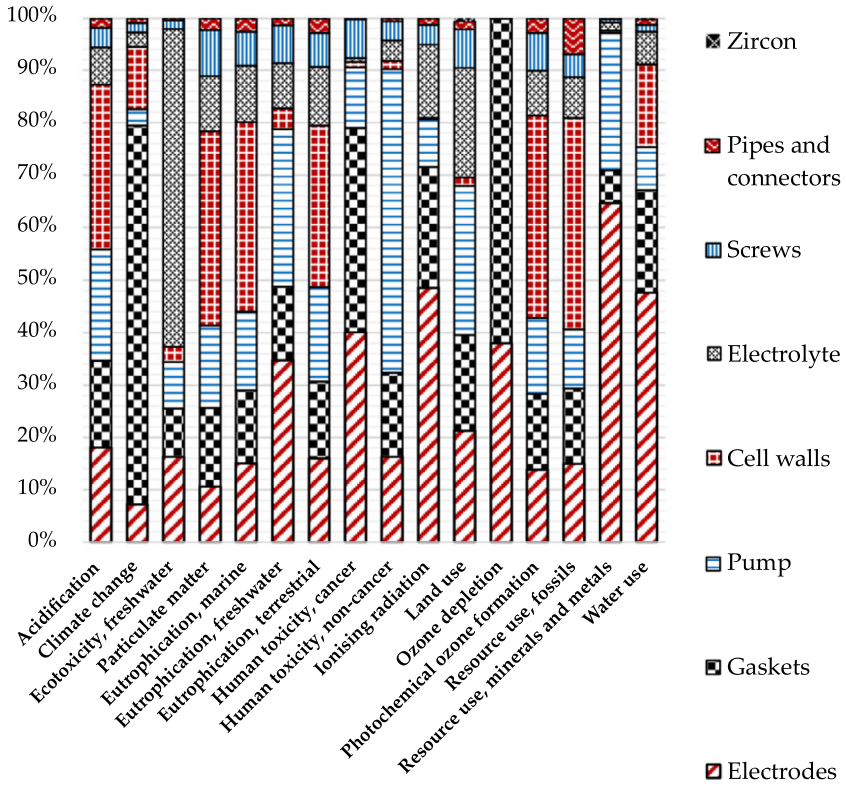

Figure 11. Contribution analysis of the cell.

Table 4. Impact assessment results for the three temperatures.

Impact categories	Unit	25 °C	40 °C	60 °C
Acidification	mol H^+_{eq}	7.96 E-05	3.44 E-04	6.18 E-04
Climate change	kg CO_{2eq}	2.01 E-02	8.71 E-02	1.56 E-01
Ecotoxicity, freshwater	CTUe	5.41 E-02	2.34 E-01	4.21 E-01
Particulate matter	kg N_{eq}	3.95 E-10	1.71 E-09	3.07 E-09
Eutrophication, marine	kg P_{eq}	1.22 E-05	5.28 E-05	9.48 E-05
Eutrophication, freshwater	mol N_{eq}	4.00 E-06	1.73 E-05	3.11 E-05
Eutrophication, terrestrial	CTUh	1.39 E-04	6.03 E-04	1.08 E-03
Human toxicity, cancer	CTUh	7.85 E-12	3.40 E-11	6.10 E-11
Human toxicity, noncancer	kBq U-235_{eq}	2.69 E-10	1.17 E-09	2.09 E-09
Ionizing radiation	Pt	2.37 E-03	1.02 E-02	1.84 E-02
Land use	kg $CFC11_{eq}$	9.12 E-02	3.95 E-01	7.08 E-01
Ozone depletion	disease inc.	4.40 E-10	1.90 E-09	3.42 E-09
Photochemical ozone formation	kg $NMVOC_{eq}$	5.82 E-05	2.52 E-04	4.52 E-04
Resource use, fossils	MJ	2.89 E-01	1.25 E+00	2.24 E+00
Resource use, minerals and metals	kg Sb_{eq}	2.13 E-07	9.23 E-07	1.66 E-06
Water use	$m^3_{depriv.}$	1.18 E-02	5.12 E-02	9.19 E-02

an increase in impact by 4.3 and 7.8 times, respectively, compared to the base case (25 °C). Results were calculated using secondary data from low-voltage electric energy produced in Italy. The considered Italian electricity mix affects the results, but even if a different mix is used (with an increasing share of renewable energy), heating the electrolyte with electric energy leads to higher energy consumption and, consequently, higher environmental impacts. While these results are not referred to an industrial-scale electrolyzer, they offer valuable insights for guiding research and design toward more sustainable solutions.

© 2025 The Author(s). ChemElectroChem published by Wiley-VCH GmbH

21960216, 0, Downloaded from https://chemistry-europe.onlinelibrary.wiley.com/doi/10.1002/celc.202500042 by University Degli Studi Di, Wiley Online Library on [26/06/2025]. See the Terms and Conditions (https://onlinelibrary.wiley.com/terms-and-conditions) on Wiley Online Library for rules of use; OA articles are governed by the applicable Creative Commons License

3. Conclusion

The results obtained in this study show that increasing the operating temperature of alkaline electrolyzers can certainly improve the performance of NiFe nanostructured electrodes. The NiFe NWs electrocatalyst exhibits promising electrocatalytic bifunctionality, showing low overpotential and optimal stability under industrial operation. In particular, really good results were obtained by operating an alkaline lab-scale electrolyzer at increasing temperatures up to 80 °C for a total of 600 h at 100 mA cm^2. However, the postcharacterization analysis indicated that Fe was etched from the surface of the NiFe NWs electrodes, particularly on the anode. Nonetheless, the NiFe NWs electrolytic cell demonstrated resilience in dynamic current conditions, suggesting its potential for industrial application. Additionally, the study examined the energy and environmental impacts of the entire alkaline cell, composed of NiFe electrodes, by applying the LCA approach. The impact assessment results indicated that the cell walls and the NiFe electrodes were responsible for the highest impact across several categories, followed by the pump, gaskets, and finally, the electrolyte. Instead, the remaining components exhibited negligible impact in nearly all considered categories. The evaluation of the impact over the 6 h operation period demonstrated that heating the electrolyte not only slightly improved cell performance but also resulted in a significant energy increase and, therefore, environmental impact. A potential alternative could involve utilizing waste heat or heat produced from renewable energy sources, such as solar thermal panels. In light of the increasing importance of hydrogen and electrolyzers, this work can serve as a starting point for further research and industrial applications, exploring alternative methods to design and heat the cell from an ecodesign perspective.

Acknowledgements

This work was partially financed by the project "SiciliAn MicronanOTecH Research And Innovation Center" "SAMOTHRACE" (MUR, PNRR-M4C2, ECS_00000022), spoke 3—Università degli Studi di Palermo "S2-COMMs—Micro and Nanotechnologies for Smart & Sustainable Communities."

Open access publishing facilitated by Universita degli Studi di Palermo, as part of the Wiley - CRUI-CARE agreement.

Conflict of Interest

The authors declare no conflict of interest.

Author Contributions

Roberto Luigi Oliveri: supervision (supporting). **Sonia longo**: investigation (equal); resources (equal). **Gabriele Miccichè**: data curation (supporting). **Nadia Moukri**: supervision (supporting). **Giuseppe Aiello**: supervision (supporting). **Maurizio Cellura**: validation (supporting). **Philippe Mandin**: supervision (supporting). **Myeongsub Kim**: supervision (equal); writing—review & editing (equal). **Rosalinda Inguanta**: data curation (equal).

Data Availability Statement

The data that support the findings of this study are available from the corresponding author upon reasonable request.

Keywords: alkaline electrolyzers · hydrogen · life cycle assessments · nanostructured electrodes · nanowires NiFe alloys

[1] S. Dresp, F. Dionigi, M. Klingenhof, P. Strasser, *ACS Energy Lett.* **2019**, *4*, 933.
[2] L. Zhuang, S. Li, J. Li, K. Wang, Z. Guan, C. Liang, Z. Xu, *Coatings* **2022**, *12*, 659.
[3] M. Chatenet, B. G. Pollet, D. R. Dekel, F. Dionigi, J. Deseure, P. Millet, R. D. Braatz, M. Z. Bazant, M. Eikerling, I. Staffell, P. Balcombe, Y. Shao-Horn, H. Schäfer, *Chem. Soc. Rev.* **2022**, *51*, 4583.
[4] J. Chi, H. Yu, *Chin. J. Catal.* **2018**, *39*, 390.
[5] A. Kudo, Y. Miseki, *Chem. Soc. Rev.* **2009**, *38*, 253.
[6] M. G. Walter, E. L. Warren, J. R. McKone, S. W. Boettcher, Q. Mi, E. A. Santori, N. S. Lewis, *Chem. Rev.* **2010**, *110*, 6446.
[7] Y. Wu, C. Sun, H. Wang, S. Ji, B. G. Pollet, J. Lu, X. Tian, H. Liang, X. Wang, R. Wang, *J. Alloys Compd.* **2022**, *903*, 163855.
[8] Y. Zhao, B. Jin, Y. Zheng, H. Jin, Y. Jiao, S. Qiao, *Adv. Energy Mater.* **2018**, *8*, 1801926.
[9] J. Zhu, L. Xia, W. Yang, R. Yu, W. Zhang, W. Luo, Y. Dai, W. Wei, L. Zhou, Y. Zhao, L. Mai, *Energy & Environ. Mater.* **2022**, *5*, 655.
[10] B. Buccheri, F. Ganci, B. Patella, G. Aiello, P. Mandin, R. Inguanta, *Electrochim. Acta* **2021**, *388*, 138588.
[11] J. Choi, A. Nkhama, A. Kumar, S. R. Mishra, F. Perez, R. K. Gupta, *Int. J. Hydrogen Energy* **2022**, *47*, 7511.
[12] S. Dresp, T. Ngo Thanh, M. Klingenhof, S. Brückner, P. Hauke, P. Strasser, *Energy Environ. Sci.* **2020**, *13*, 1725.
[13] S. Kumaravel, K. Karthick, S. Sam Sankar, A. Karmakar, R. Madhu, K. Bera, S. Kundu, *ChemElectroChem* **2021**, *8*, 4638.
[14] A. N. Colli, H. H. Girault, A. Battistel, *Materials* **2019**, *12*, 1336.
[15] C. Kuai, Z. Xu, C. Xi, A. Hu, Z. Yang, Y. Zhang, C.-J. Sun, L. Li, D. Sokaras, C. Dong, S.-Z. Qiao, X.-W. Du, F. Lin, *Nat. Catal.* **2020**, *3*, 743.
[16] R. Chen, S. Hung, D. Zhou, J. Gao, C. Yang, H. Tao, H. B. Yang, L. Zhang, L. Zhang, Q. Xiong, H. M. Chen, B. Liu, *Adv.Mater* **2019**, *31*, 1903909.
[17] K. Khan, A. K. Tareen, M. Aslam, Y. Zhang, R. Wang, Z. Ouyang, Z. Gou, H. Zhang, *Nanoscale* **2019**, *11*, 21622.
[18] M. P. Browne, Z. Sofer, M. Pumera, *Energy Environ. Sci.* **2019**, *12*, 41.
[19] S. H. Ahn, I. Choi, H.-Y. Park, S. J. Hwang, S. J. Yoo, E. Cho, H.-J. Kim, D. Henkensmeier, S. W. Nam, S.-K. Kim, J. H. Jang, *Chem. Commun.* **2013**, *49*, 9323.
[20] M. L. Frederiksen, R. C. Oglou, J. V. Lauritsen, A. Bentien, L. P. Nielsen, *Electrochim. Acta* **2024**, *482*, 143988.
[21] S. Jin, *ACS Energy Lett.* **2017**, *2*, 1937.
[22] D. Hochfilzer, I. Chorkendorff, J. Kibsgaard, *ACS Energy Lett.* **2023**, *8*, 1607.
[23] R. Gilliam, J. Graydon, D. Kirk, S. Thorpe, *Int. J. Hydrogen Energy* **2007**, *32*, 359.
[24] X. Lyu, J. Li, J. Yang, A. Serov, *J. Environ. Chem. Eng.* **2023**, *11*, 111492.
[25] P. M. Diéguez, A. Ursúa, P. Sanchis, C. Sopena, E. Guelbenzu, L. M. Gandía, *Int. J. Hydrogen Energy* **2008**, *33*, 7338.
[26] E. Amores, J. Rodríguez, C. Carreras, *Int. J. Hydrogen Energy* **2014**, *39*, 13063.
[27] D. Jang, W. Choi, H.-S. Cho, W. C. Cho, C. H. Kim, S. Kang, *J. Power Sources* **2021**, *506*, 230106.
[28] D. M. Sayed, G. A. El-Nagar, S. Y. Sayed, B. E. El-Anadouli, M. S. El-Deab, *Electrochim. Acta* **2018**, *276*, 176.
[29] G. Zhang, H. Wang, J. Yang, Q. Zhao, L. Yang, H. Tang, C. Liu, H. Chen, Y. Lin, F. Pan, *Inorg. Chem.* **2018**, *57*, 2766.
[30] G. Shi, T. Tano, D. A. Tryk, M. Yamaguchi, A. Iiyama, M. Uchida, K. Iida, C. Arata, S. Watanabe, K. Kakinuma, *ACS Catal.* **2022**, *12*, 14209.
[31] S. Carbone, F. Proietto, F. Bonafede, R. L. Oliveri, B. Patella, F. Ganci, G. Aiello, P. Mandin, M. Kim, M. Scopelliti, R. Inguanta, *Electrochim. Acta* **2023**, *467*, 143120.

© 2025 The Author(s). ChemElectroChem published by Wiley-VCH GmbH

21960216, 0, Downloaded from https://chemistry-europe.onlinelibrary.wiley.com/doi/10.1002/celc.202500042 by University Degli Studi Di, Wiley Online Library on [26/06/2025]. See the Terms and Conditions (https://onlinelibrary.wiley.com/terms-and-conditions) on Wiley Online Library for rules of use; OA articles are governed by the applicable Creative Commons License

[32] M. S. Tovar-Oliva, I. Tudela, *Res. Eng.* **2024**, *24*, 103285.
[33] A. Serrà, E. Vallés, *Appl. Mater. Today* **2018**, *12*, 207.
[34] N. Yang, H. Li, J. Hao, X. Lin, S. Kondrat, C. Hardacre, W.-F. Lin, *Curr. Opin. Electrochem.* **2024**, *47*, 101566.
[35] P. Sebastián-Pascual, I. Jordão Pereira, M. Escudero-Escribano, *Chem. Commun.* **2020**, *56*, 13261.
[36] European Commission - Joint Research Centre, EN 15804 reference package based on EF 3.1 reference package **2023**.
[37] J. R. Macdonald, C. A. Barlow, *J. Chem. Phys.* **1962**, *36*, 3062.
[38] A. J. Bard, L. L. Faulkner, H. S. White, *Electrochemical Methods: Fundamentals And Applications*, *3rd Edition*,published by Wiley-Blackwell, ISBN: 9781119334057, Editorial Office 9600 Garsington Road, Oxford, OX4 2DQ, UK **2022**.
[39] C. C. L. McCrory, S. Jung, I. M. Ferrer, S. M. Chatman, J. C. Peters, T. F. Jaramillo, *J. Am. Chem. Soc.* **2015**, *137*, 4347.
[40] F. Rocha, R. Delmelle, C. Georgiadis, J. Proost, *J. Environ. Chem. Eng.* **2022**, *10*, 107648.
[41] F. Ganci, S. Lombardo, C. Sunseri, R. Inguanta, *Renew. Energy* **2018**, *123*, 117.
[42] F. Ganci, T. Baguet, G. Aiello, V. Cusumano, P. Mandin, C. Sunseri, R. Inguanta, *Energies* **2019**, *12*, 3669.
[43] M. B. Stevens, L. J. Enman, A. S. Batchellor, M. R. Cosby, A. E. Vise, C. D. M. Trang, S. W. Boettcher, *Chem. Mater.* **2017**, *29*, 120.
[44] J. Barco-Burgos, U. Eicker, N. Saldaña-Robles,A. L. Saldaña-Robles, V. Alcántar-Camarena, *Fuel*, **2020**, *276*, 117910.
[45] M. Schalenbach, A. R. Zeradjanin, O. Kasian, S. Cherevko, K. J. J. Mayrhofer, *Int. J. Electrochem. Sci.* **2018**, *13*, 1173.
[46] A. Raveendran, M. Chandran, R. Dhanusuraman, *RSC Adv.* **2023**, *13*, 3843.
[47] S. Marini, P. Salvi, P. Nelli, R. Pesenti, M. Villa, M. Berrettoni, G. Zangari, Y. Kiros, *Electrochim. Acta* **2012**, *82*, 384.
[48] N. Nagai, *Int. J. Hydrogen Energy* **2003**, *28*, 35.
[49] M. Matlosz, *J. Electrochem. Soc.* **1993**, *140*, 2272.
[50] T.-R. Lee, L. Chang, C.-H. Chen, *Surf. Coat. Technol.* **2012**, *207*, 523.
[51] K.-M. Yin, B.-T. Lin, *Surf. Coat. Technol.* **1996**, *78*, 205.
[52] O. Dragos, H. Chiriac, N. Lupu, M. Grigoras, I. Tabakovic, *J. Electrochem. Soc.* **2016**, *163*, D83.
[53] L. Liu, J. Guan, W. Shi, Z. Sun, J. Zhao, *J. Phys. Chem. C* **2010**, *114*, 13565.
[54] ISO 14040, Environmental Management: Life Cycle Assessment; Principles and Framework **2021**.
[55] ISO 14044, Environmental Management: Life Cycle Assessment; Requirements and Guidelines **2021**.
[56] B. Steubing, G. Wernet, J. Reinhard, C. Bauer, E. Moreno-Ruiz, *Int J. Life Cycle Assess* **2016**, *21*, 1269.

Manuscript received: January 30, 2025
Revised manuscript received: April 16, 2025
Version of record online:

© 2025 The Author(s). ChemElectroChem published by Wiley-VCH GmbH

21960216, 0, Downloaded from https://chemistry-europe.onlinelibrary.wiley.com/doi/10.1002/celc.202500042 by University Degli Studi Di, Wiley Online Library on [26/06/2025]. See the Terms and Conditions (https://onlinelibrary.wiley.com/terms-and-conditions) on Wiley Online Library for rules of use; OA articles are governed by the applicable Creative Commons License